Cell Reports

Supplemental Information

Telomerase Is Essential for Zebrafish Heart Regeneration

Dorota Bednarek, Juan Manuel González-Rosa, Gabriela Guzmán-Martínez, Óscar Gutiérrez-Gutiérrez, Tania Aguado, Carlota Sánchez-Ferrer, Inês João Marques, María Galardi-Castilla, Irene de Diego, Manuel José Gómez, Alfonso Cortés, Agustín Zapata, Luis Jesús Jiménez-Borreguero, Nadia Mercader, and Ignacio Flores

Supplemental Information Inventory

Telomerase is essential for zebrafish heart regeneration

-Supplemental Figures and Supplemental Figure Legends (from Figure S1 to Figure S7)

Figure S1. Inflammatory response in cryoinjured *tert*$^{-/-}$ zebrafish hearts. Related to Figure 2.

Figure S2. Early activation of epicardial and endocardial genes is unaffected in the absence of telomerase. Related to Figure 2.

Figure S3. Cardiomyocyte dedifferentiation is unaffected in the absence of telomerase. Related to Figure 2.

Figure S4. *tert* loss of function leads to reduced cardiomyoyte proliferation. Related to Figure 3.

Figure S5. *tert* silencing in the injured hearts inhibits the proliferative response of cardiac cells. Related to Figure 3.

Figure S6. Telomere length dynamics of cardiac cells and location of proliferating WT cardiomyocytes in the non-injured and cryoinjured heart. Related to Figure 4 and 5.

Figure S7. Cardiac cells with accumulated DNA damage are less prone to proliferate. Related to Figure 6.

-Supplemental Movies and Supplemental Movie Legends (from Movie S1 to Movie S6)

Movie S1. Doppler echocardiography recording of an uninjured wildtype zebrafish heart. Related to Figure 2.

Movie S2. Doppler echocardiography recording of an uninjured *tert*$^{-/-}$ zebrafish heart. Related to Figure 2.

Movie S3. Doppler echocardiography recording of a wildtype zebrafish heart at 3 dpi. Related to Figure 2.

Movie S4. Doppler echocardiography recording of a *tert*$^{-/-}$ zebrafish heart at 3 dpi. Related to Figure 2.

Movie S5. Doppler echocardiography recording of a wildtype zebrafish heart at 60 dpi. Related to Figure 2.

Movie S6. Doppler echocardiography recording of a *tert*$^{-/-}$ zebrafish heart at 60 dpi. Related to Figure 2.

Supplemental Table S1. Related to Figure 2.

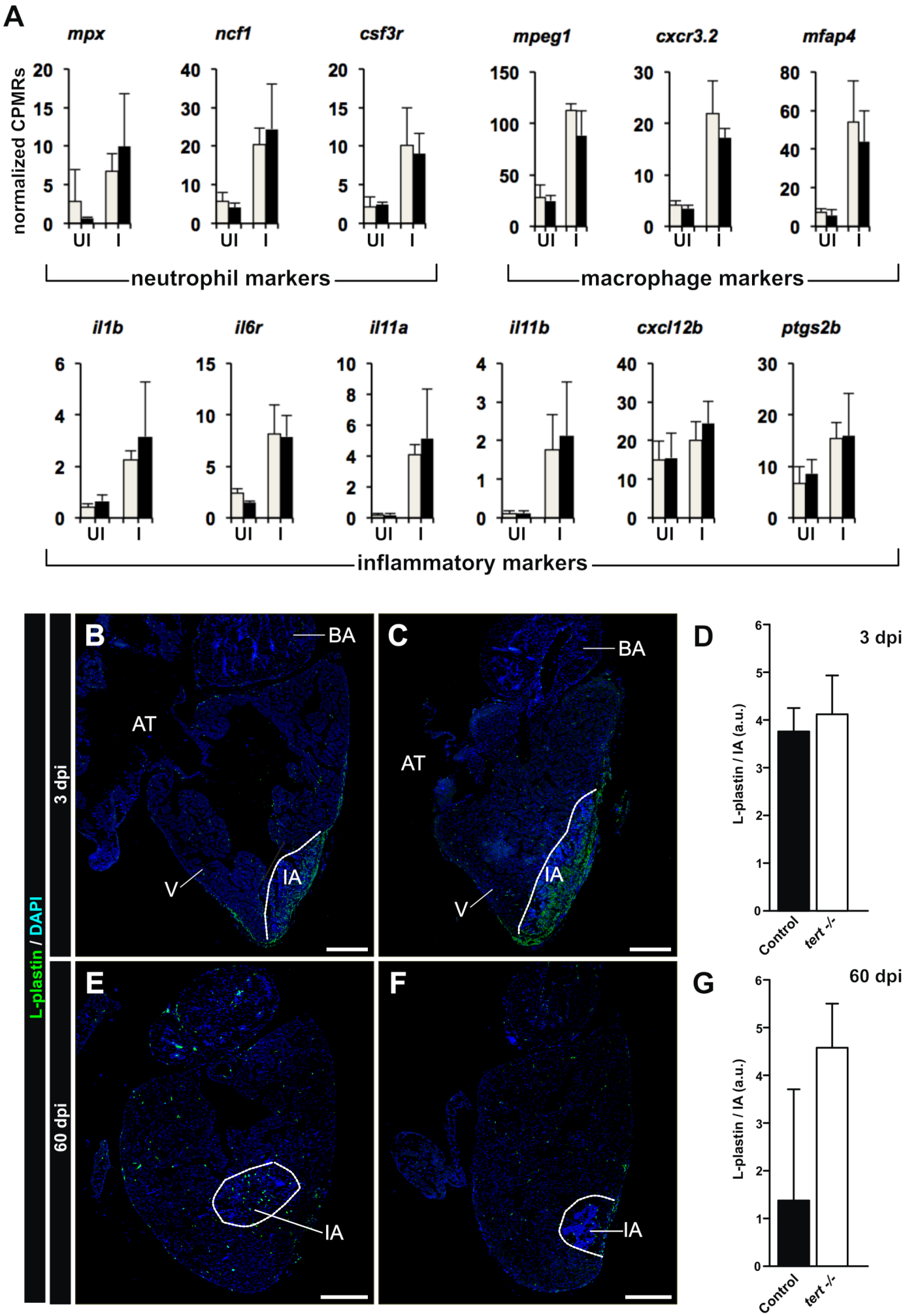

Bednarek et al,
Supplementary Figure 1

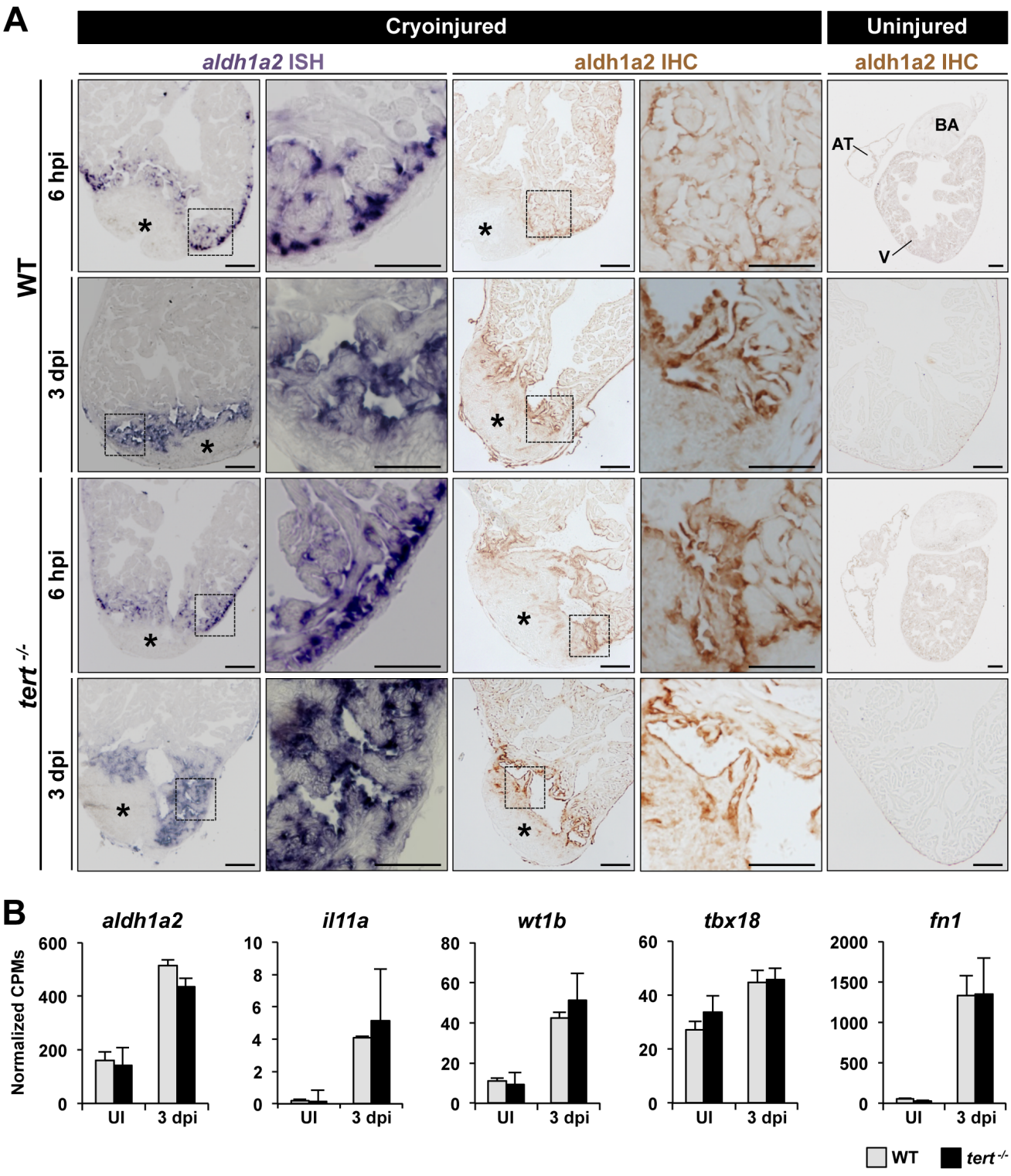

Bednarek *et al.*
Supplementary Figure 2

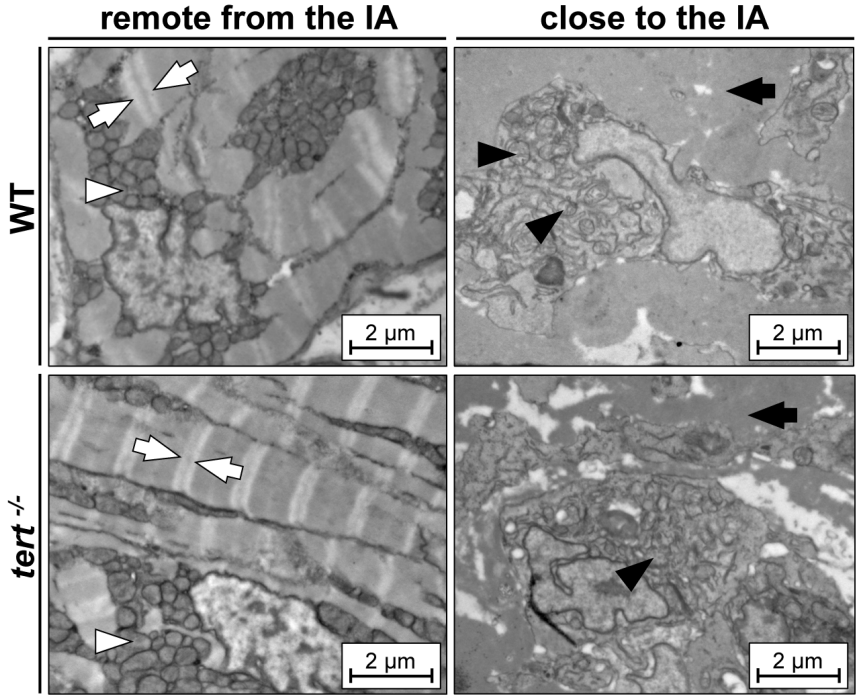

Bednarek *et al.*
Supplementary Figure 3

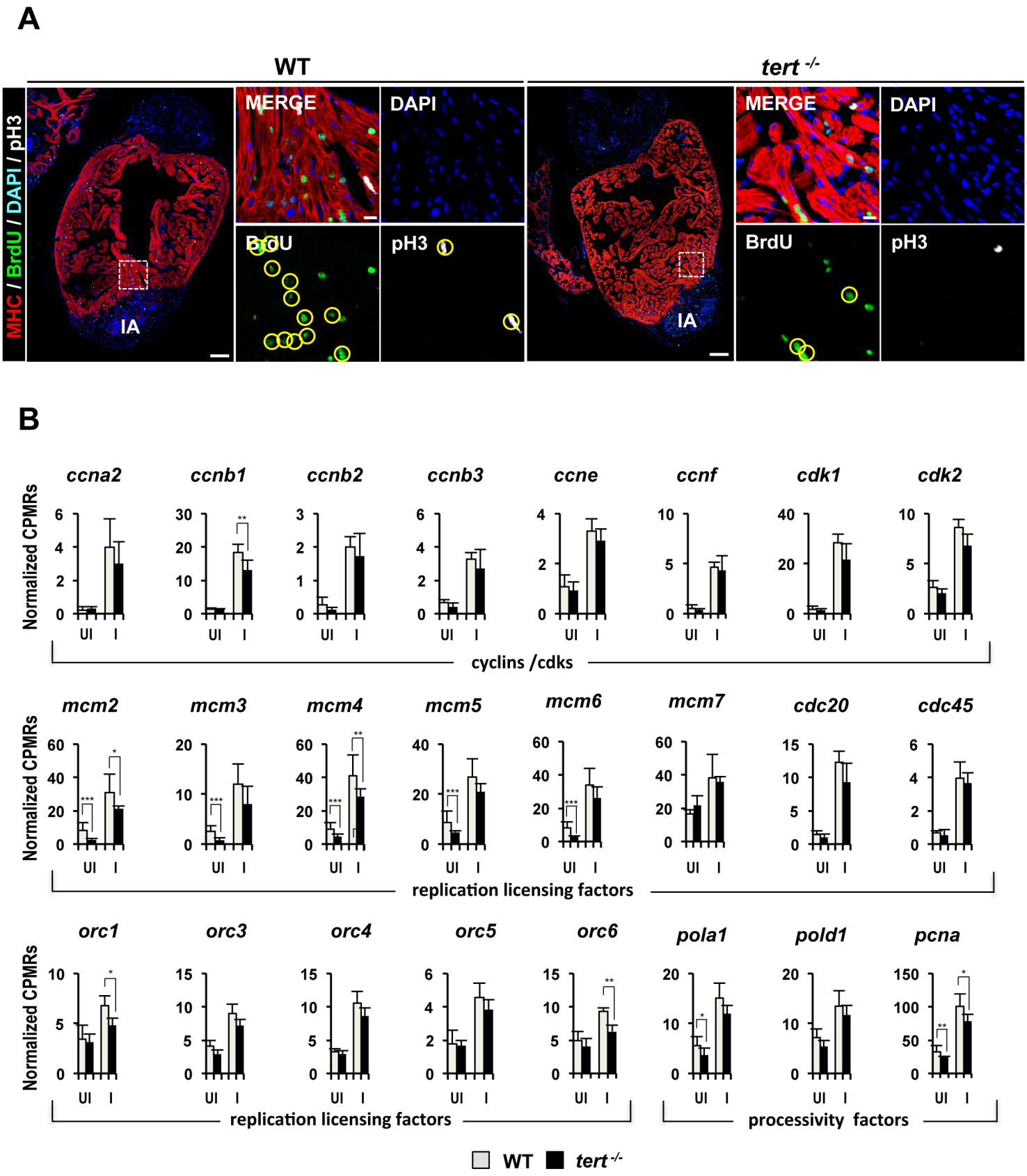

Bednarek *et al.*
Supplementary Figure 4

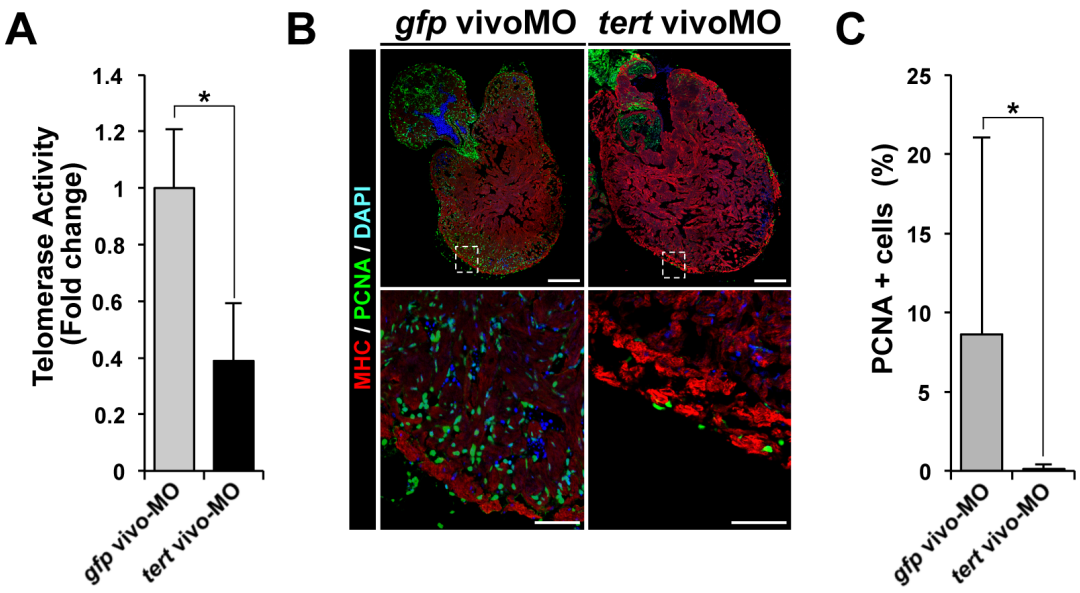

Bednarek *et al.*
Supplementary Figure 5

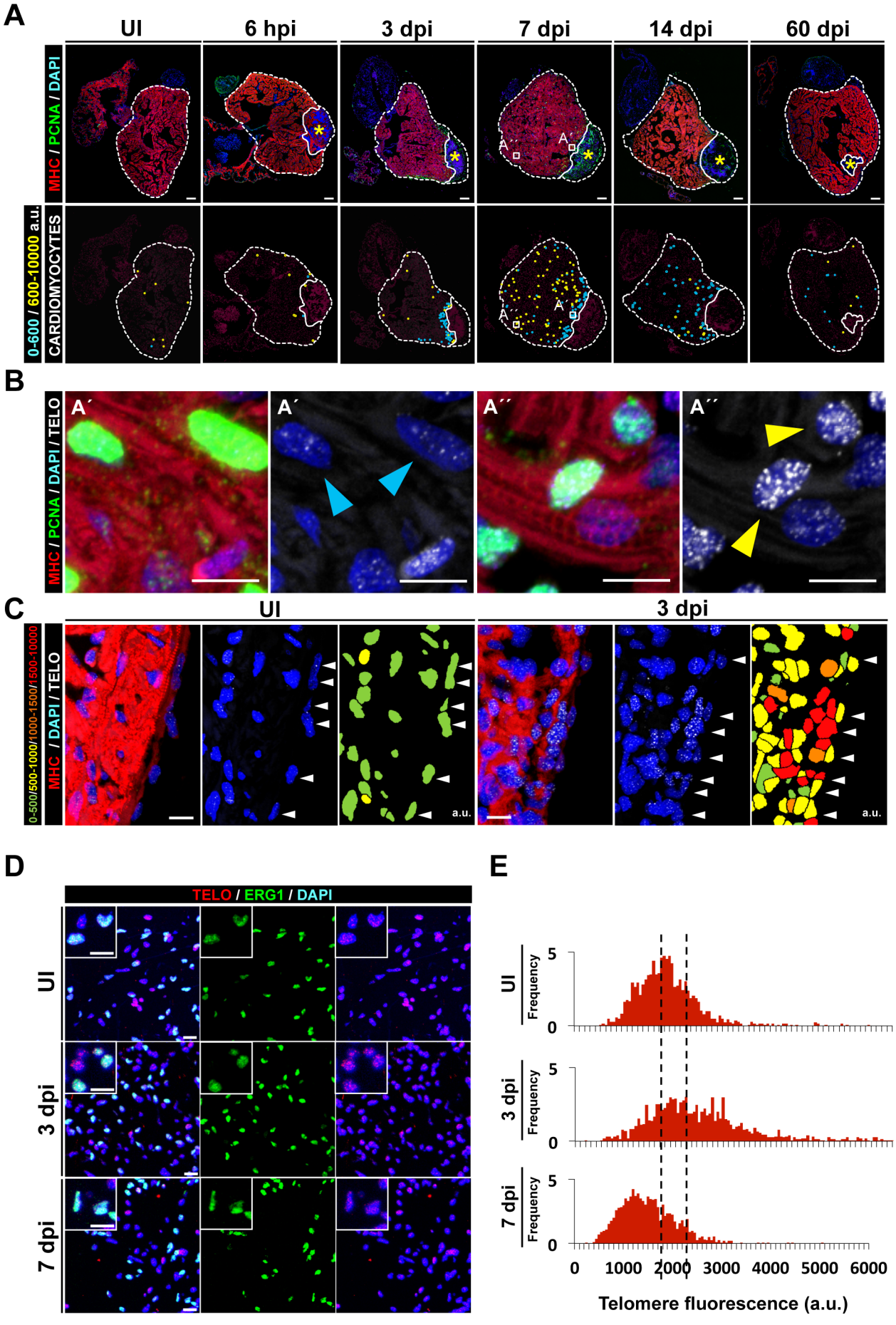

Bednarek *et al.*
Supplementary Figure 6

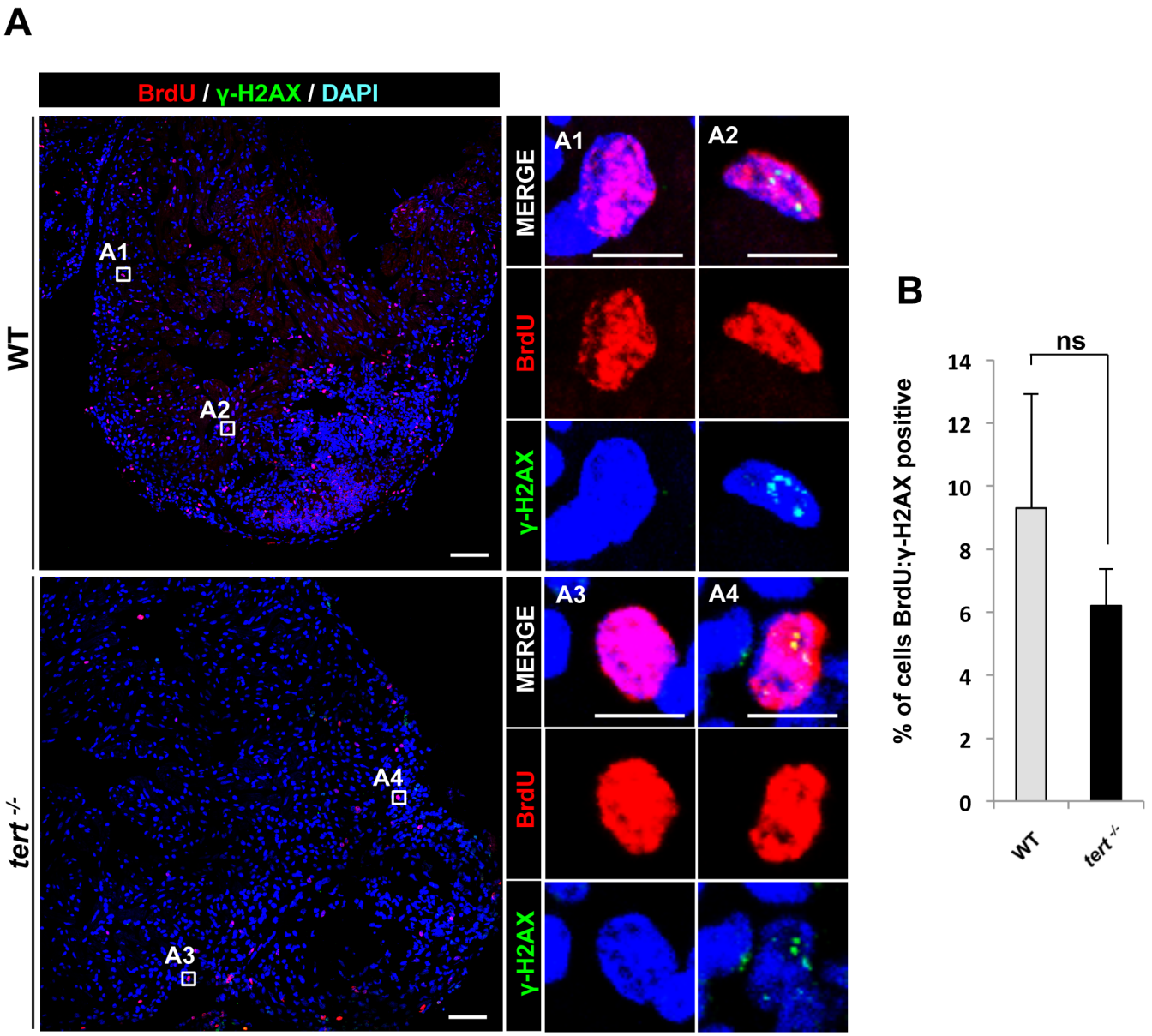

Bednarek *et al.*
Supplementary Figure 7

Telomerase is essential for zebrafish heart regeneration

Supplemental Figure Legends

Figure S1. Inflammatory response in cryoinjured *tert*$^{-/-}$ zebrafish hearts.
(A) RNA expression of neutrophil, macrophage and inflammatory marker genes in wildtype (WT, grey bars) and *tert*$^{-/-}$ zebrafish hearts (black bars), uninjured or 3 days postinjury (dpi). Injury led to an increase in the expression of the markers analyzed both in WT and *tert*$^{-/-}$ hearts. Differences between WT and *tert*$^{-/-}$ zebrafish hearts are non-significant in all cases (B-H adjusted p-value). Data are means ± SEM of values obtained from an RNA-seq experiment of 4 biological replicates, each replicate consisting of 3 pooled hearts. CPM, counts per million; dpi, days postinjury; I, injured; UI, uninjured.

(B-G) Immunofluorescence of L-plastin (green) on WT (B,E) and *tert*$^{-/-}$ (C,F) heart sections and the quantification of L-plastin positive cells at 3 (B-D) and 60 dpi (E-G). DAPI was used to counterstain nuclei (blue). Graphs show means ± SEM L-plastin signal in the injured area (IA) and within 50 µm of the border zone on sections from 3 hearts per condition. The IA is outlined by a dotted line. AT, atrium; a.u. arbitrary units; BA, bulbus arteriosus; dpi, days postinjury; IA, injured area; V, ventricle. Bars, 200 µm.

Related to Figure 2.

Figure S2. Early activation of epicardial and endocardial genes is unaffected in the absence of telomerase.
(A) Representative images of *aldh1a2* RNA and protein expression detected by *in situ* hybridization (ISH) and immunohistochemistry (IHC) in endocardium and epicardium at the indicated times post-injury in WT and *tert*$^{-/-}$ zebrafish hearts. IHC on uninjured heart sections are shown for comparison. A total of n=4 hearts were analyzed per condition, with a minimum of 3 analyzed sections per heart. Asterisks mark the injured region. Boxed areas are shown at higher magnification. At, atrium; BA, bulbus arteriosus; dpi, days postinjury; V, ventricle. Scale bars: 100 µm for general views and 50 µm for zoomed views.

(B) RNA expression of endocardial genes (*aldh1a2, il11a*) and epicardial genes (*wt1b, tbx18 and fibronectin)* upregulated upon cardiac injury in WT and *tert*$^{-/-}$ zebrafish hearts. Data are means ± SEM of values obtained from an RNA-seq experiment of 4 biological replicates, each replicate consisting of a pool of 3 hearts. Differences between WT and *tert*$^{-/-}$ zebrafish hearts are non-significant in all cases (B-H adjusted p-value). CPM, counts per million; dpi, days postinjury; UI, uninjured.

Related to Figure 2.

Figure S3. Cardiomyocyte dedifferentiation is unaffected in the absence of telomerase.

Transmission electron micrographs of cardiomyocytes at 3 days post injury. (Left) Representative cardiomyocytes away from the injury site in WT and *tert*$^{-/-}$ animals, showing ordered sarcomeric fibers with visible Z-lines (white arrows) and perinuclear mitochondria with typical structure (white arrowheads). (Right) Representative cardiomyocytes close to the injury site, showing disorganized sarcomeric structure with loss of Z-lines (black arrows) and dysmorphic mitochondria (black arrowheads). IA, injury area; WT, wildtype. Scale bars: 2 µm.

Related to Figure 2.

Figure S4. *tert* loss of function leads to reduced cardiomyoyte proliferation. (A) Immunofluorescence staining on wildtype (WT) and *tert*$^{-/-}$ hearts with anti-myosin heavy chain (MHC, red), anti-BrDU (green) and anti-phospho histone 3 (pH3, white). Nuclei are counterstained with DAPI. Boxed areas are shown at higher magnification; yellow circles highlight BrdU/MHC and pH3/MHC double positive cardiomyocytes. Note that fewer pH3 and BrdU-positive cardiomyocytes are found in the *tert*$^{-/-}$ heart. Scale bars: 100 µm (whole mount views), 10 µm (magnifications).

(B) RNA expression of cyclins, cdks, replication licensing factors and processivity factors implicated in a proliferation response in uninjured and 3 dpi WT and *tert*$^{-/-}$ hearts. Data are means ± SEM of values obtained from an RNA-seq experiment of 4 biological replicates, each replicate consisting of 3 pooled hearts. CPM, counts per million; dpi, days postinjury. *p<0.05, ** p<0.01, *** p<0.001 (Benjamini-Hochberg adjusted p-values).

Related to Figure 3.

Figure S5. *tert* silencing in the injured hearts inhibits the proliferative response of cardiac cells.

(A) tert activity assay in stab-injured hearts cultured for 3 days in the presence of 10 μM *gfp* vivo Morpholino or *tert* vivo Morpholino. Data are means ± SD from 2 pools of 3 hearts per condition ($p<0.05$, unpaired Student's t-test). A second experiment using 2 additional control and *tert* vivoMO replicates at 15 μM (3 pooled hearts per replicate) yielded the same result (data not shown).

(B) Immunfluorescence analysis of *gfp* and *tert* vivoMO-treated hearts. Stab-injured hearts were immunostained for PCNA (green) and myosin heavy chain (MHC, red), and nuclei were counterstained with DAPI (blue). Boxed areas are shown at higher magnification in the lower panels. Bars, 200 μm (whole heart images), 50 μm (zoomed views).

(C) Quantification of the percentage of PCNA-positive cells per total cell nuclei in hearts treated with *gfp* or *tert* vivoMO. Data are means ± SD from 4-5 hearts per condition ($p<0.05$, unpaired Student's t-test).

Related to Figure 3.

Figure S6. Telomere length dynamics of cardiac cells and location of proliferating WT cardiomyocytes in the non-injured and cryoinjured heart.

(A) The top row shows representative sections of zebrafish hearts immunostained for the cardiomyocyte marker MHC (red) and the proliferation marker PCNA (green), with nuclear counterstaining with DAPI (blue). Asterisks mark the injured area. The bottom row shows the locations of proliferating cardiomyocytes. The panels depict proliferating cardiomyocytes with relatively short telomeres (<600 a.u.) in light blue and those with relatively long telomeres (> 600 a.u.) in yellow.

(B) Representative proliferating cardiomyocytes located close to the injury site (A´) and in the remote region (A´´). Arrowheads indicate PCNA-positive cardiomyocytes with short (blue arrowhead) or long (yellow arrowhead) telomeres.

(C) Telomere length dynamics in the epicardium region of uninjured and 3 dpi WT zebrafish hearts. White arrowheads indicate epicardial cells.

(D) Immunostaining of the endocardium (endothelial cell marker erg1; green) combined with Q-FISH detection of telomere length (red) in uninjured, 3 dpi and 7 dpi WT zebrafish hearts. Nuclei are counterstained with DAPI (blue).

(E) Representative histograms showing the frequency of telomere fluorescence in arbitrary units (a.u.) in endocardial cells upon cryoinjury.

a.u. arbitrary units; dpi, days postinjury; hpi; hours postinjury; PCNA, proliferating nuclear cell antigen; WT, wildtype. Scale bars: 100 μm for whole heart sections and 10 μm for zooms.

Related to Figure 4 and 5.

Figure S7. Cardiac cells with accumulated DNA damage are less prone to proliferate.

(A) Immunofluorescence staining on a WT and a *tert*$^{-/-}$ heart section with anti-BrdU (red) and anti-γH2AX (green). Nuclei are counterstained with DAPI (blue). (A1-A4) Boxed areas in the whole-mount heart views of WT (A1,A2) and *tert*$^{-/-}$ (A3,A4) are shown at high magnification in the right panels to exemplify individual BrDU-positive cells. Scale bars: 100 μm (whole mount views), 10 μm (magnifications).

(B) Quantification of cells double positive for BrDU and γH2AX. Data are means ± SEM of 4 sections/heart from a total of 3 hearts per condition (p=0.106, unpaired Student's t-test). ns, not significant.

Related to Figure 6.

Movie S1. Doppler echocardiography recording of an uninjured wildtype zebrafish heart. Ventricle long axis: the head of the fish is to the right; ventral side is upwards. Red and blue areas indicate blood. The movie was acquired at 48 Hz. Related to Figure 2.

Movie S2. Doppler echocardiography recording of an uninjured *tert*$^{-/-}$ zebrafish heart. Ventricle long axis: the head of the fish is to the right; ventral side is upwards. Red and blue areas indicate blood. The movie was acquired at 48 Hz. Related to Figure 2.

Movie S3. Doppler echocardiography recording of a wildtype zebrafish heart at 3 dpi. Ventricle long axis: the head of the fish is to the right; ventral side is upwards. Red and blue areas indicate blood. Note the smaller colored area compared to the uninjured heart in Movie S1, indicating lower ventricular pumping efficiency. The movie was acquired at 48 Hz. Related to Figure 2.

Movie S4. Doppler echocardiography recording of a *tert*$^{-/-}$ zebrafish heart at 3 dpi. Ventricle long axis: the head of the fish is to the right; ventral side is upwards. Red and blue areas indicate blood. Note the smaller colored area compared to the uninjured heart in Movie S2, indicating lower ventricular pumping efficiency. The movie was acquired at 48 Hz. Related to Figure 2.

Movie S5. Doppler echocardiography recording of a wildtype zebrafish heart at 60 dpi. Ventricle long axis: the head of the fish is to the right; ventral side is upwards. Red and blue areas indicate the blood. The movie was acquired at 48 Hz. Related to Figure 2.

Movie S6. Doppler echocardiography recording of a *tert*$^{-/-}$ zebrafish heart at 60 dpi. Ventricle long axis: the head of the fish is to the right; ventral side is upwards. Red and blue areas indicate blood. Note the smaller colored area compared to the wildtype heart at 60 dpi in Movie S5, indicating non- recovery of ventricular pumping

Gene set	WT I vs. UI	*tert* $^{-/-}$ I vs. UI	UI WT vs. *tert* $^{-/-}$	I WT vs. *tert* $^{-/-}$
Proliferation				
BioCarta: cell cycle pathway	I	I	n.s.	WT
KEGG: cell cycle	I	I	WT	WT
Reactome: cell cycle checkpoints	I	I	WT	n.s.
Reactome: cell cycle mitotic	I	I	WT	WT
Reactome: cell cycle	I	I	WT	WT
Reactome: regulation of mitotic cell cycle	I	I	n.s.	n.s.
Reactome: S phase	I	I	WT	n.s.
Inflammation				
BioCarta: cytokine pathway	n.s.	n.s.	n.s.	n.s.
BioCarta: inflammation pathway	n.s.	n.s.	n.s.	n.s.
KEGG: cytokine cytokine-receptor interaction	I	I	n.s.	n.s.
KEGG: Jak-Stat signaling pathway	n.s.	I	n.s.	n.s.
KEGG: T-cell receptor signaling pathway	I	I	n.s.	n.s.
Reactome: cytokine signaling in immune system	I	I	n.s.	n.s.
Reactome: signaling by ILs	I	I	n.s.	n.s.

Table S1. Bioinformatics analysis of the effect of *tert* loss-of-function on cell proliferation and inflammation. RNA-seq experiments were performed with heart samples from uninjured (*UI*) or 3 dpi (cryoinjured, *I*) wildtype (WT) and *tert* $^{-/-}$ zebrafish. The resulting expression profiles were compared by GSEA (Subramanian et al., 2005) to assess the effect of *tert* loss-of-function on a collection of gene sets that represent signaling pathways related to cell proliferation and inflammation, extracted from the Molecular Signatures Database (Subramanian et al, 2005). For each of the comparisons performed, the table indicates the condition in which upregulated genes of any of the given gene sets were significantly enriched (FDR q-value < 0.05) relative to the other condition (*n.s.*, no significant enrichment in any condition). WT heart expression profiles were enriched in upregulated genes belonging to pathways involved in cell proliferation, but not inflammation, regardless of the treatment (cryoinjured, uninjured). In contrast, cryoinjured heart expression profiles revealed a consistent enrichment in upregulated genes belonging to gene sets related both to cell proliferation and inflammation, irrespective of the genetic background (WT, *tert* $^{-/-}$).

Reference: Subramanian, A., Tamayo, P., Mootha, V.K., Mukherjee, S., Ebert, B.L., Gillette, M.A., Paulovich, A., Pomeroy, S.L., Golub, T.R., Lander, E.S.*, et al.* (2005). Gene set enrichment analysis: a knowledge-based approach for interpreting genome-wide expression profiles. Proceedings of the National Academy of Sciences of the United States of America *102*, 15545-15550.